International Journal of Mechanical, Industrial and Aerospace Sciences
ISSN: 2517-9950
Vol:10, No:2, 2016

Thrust Enhancement on a Two Dimensional Elliptic Airfoil in a Forward Flight

S. M. Dash, K. B. Lua, T. T. Lim

***Abstract*—**This paper presents results of numerical and experimental studies on a two-dimensional (2D) flapping elliptic airfoil in a forward flight condition at Reynolds number of 5000. The study is motivated from an earlier investigation which shows that the deterioration in thrust performance of a sinusoidal heaving and pitching 2D (NACA0012) airfoil at high flapping frequency can be recovered by changing the effective angle of attack profile to square wave, sawtooth, or cosine wave shape. To better understand why such modifications lead to superior thrust performance, we take a closer look at the transient aerodynamic force behavior of an airfoil when the effective angle of attack profile changes gradually from a generic smooth trapezoidal profile to a sinusoid shape by modifying the base length of the trapezoid. The choice of using a smooth trapezoidal profile is to avoid the infinite acceleration condition encountered in the square wave profile. Our results show that the enhancement in the time-averaged thrust performance at high flapping frequency can be attributed to the delay and reduction in the drag producing valley region in the transient thrust force coefficient when the effective angle of attack profile changes from sinusoidal to trapezoidal.

***Keywords*—**Two-dimensional Flapping Airfoil, Thrust Performance, Effective Angle of Attack, CFD and Experiments.

I. Introduction

THE study of the aerodynamics of a pitching and plunging airfoil is relevant to many engineering applications including Micro-Air-Vehicles (MAVs) and Under-Water-Vehicles (UWVs) which mimics natural flyers or swimmers [1]-[7]. Past studies [1]-[5] have shown that thrust producing conditions of an oscillating airfoil is associated with jet-like flow structures downstream of the airfoil where the vortices are arranged to produce momentum excess. Triantafyllou et al. [6], [7] characterized the thrust performance of flapping foil in terms of flapping frequency (*f*) or Strouhal number (S_T). In subsequent studies [8], [9], it was found that although higher flapping frequency produced higher time-average thrust, there exists a critical Strouhal number (S_{Tc}), above which thrust performance of a sinusoidal heaving and pitching airfoil deteriorated considerably. In [10], it was found that the deterioration in thrust performance is linked to the transient thrust force profile switching from a single peak parabolic-like shape to drag producing multiple peaks non-parabolic type in one flapping stroke; i.e. upstroke or downstroke. In this paper, we extended our investigation to determine if thrust performance can be further improved by reducing the drag producing valley region in the multiple-peak transient thrust force profile when the Strouhal number (S_T) is above the critical value of S_{Tc}.

In a related past experiment by [9] on a 2D oscillating NACA0012 airfoil at Re=30,000 and S_T varying from 0.2 to 0.8, it was found that modifying the instantaneous effective angle of attack profile from sinusoidal to cosine, sawtooth or square-wave type can lead thrust enhancement. Subsequent numerical simulations by [11] and [12] further confirmed the findings of [9]. Although the past studies have provided some valuable insights into the salient factors responsible for the thrust enhancement, the details are still not fully understood. The attempt by [9] to relate the thrust enhancement to changes in the far field wake topology, although useful, is indicative of the mean thrust only; it does not give much insight into the temporal thrust behavior. To address this issue, we systematically investigate how changes in the effective angle of attack profile influence the transient and time-average thrust of flapping foil. Here, we focus on a smooth trapezoidal effective angle of attack profile and vary the base length of the trapezoid until it eventually transforms into a sinusoidal wave.

The present study consisted of both experimental and numerical investigations using a 2D elliptic airfoil. The experiments were conducted in a water channel using the flapping airfoil mechanism previously used by [13]. The numerical simulations were conducted using a commercial CFD package (FLUENT v15.0) with laminar viscous flow model. The simulation was conducted on at Re=5000, S_T from 0.1 to 0.8 and induced effective angle of attack amplitude (α_0) from 10^0 to 20^0.

The reminder of the paper is arranged as follows. Section II presents the experimental setup and methodology. Section III discusses the numerical scheme, problem definition, and validation of the CFD solver. Results are discussed in Section IV, and some concluding remarks are drawn in Section V.

II. Experimental Set up and Procedure

The experiments were conducted in a re-circulating water channel as shown in Fig. 1, where the flapping wing mechanism was placed on top of its test section. The linear translation (heaving) of the elliptic airfoil was controlled by a Mdrive23 stepper motor with fine resolution of 0.005 mm and the rotation (pitching) motion was controlled by a second Mdrive23 stepper motor with resolution of 0.018 deg. Although complete elimination of the vibration from discrete micro-stepping action of the motor is impossible, various measures were adopted to ensure that the vibration was kept to a very minimum level, such that the flow field is unaffected. This minimal level of vibration was encountered by [13] in a

Sunil Manohar Dash is with the National University of Singapore, Singapore (e-mail: mpedsm@nus.edu.sg).

related investigation on the vortex shedding process of a 2D flapping elliptic wing in a free stream where they found good agreement between their experimental results and the computation of [2].

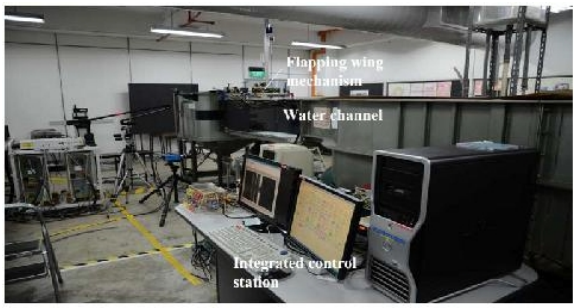

(a)

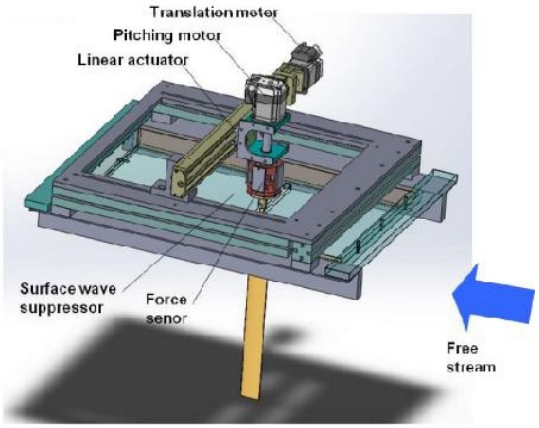

(b)

Fig. 1 (a) Two dimensional flapping airfoil setup with (b) details of flapping mechanism

The elliptic airfoil used in the study has a length (L) of 0.4 m, chord (c) of 0.04 m and maximum thickness (t) of 0.005 m. Accordingly, the aspect ratio of the airfoil (L/c) was 10, which was much higher than the critical aspect ratio limit [13]-[15] (<1:5) to minimize three dimensional effect. To further avoid the influence of the wing tip vortices, the elliptic airfoil was bounded in between two perspex (or plexiglas) endplates. The top endplate was placed on the water surface, which also prevented free surface effects. The base plate of the water tunnel served as the bottom endplate, where the gap was less than 0.002 m.

The force measurement system used in the present study consisted of a two-component force sensor, a Wheatstone bridge, a Butterworth filter, and a PC installed with a data acquisition (A/D) card. The force sensor has four bending bars, where strain gauges were affixed to all the sixteen surfaces of the bars. The measured analog signals were then low-pass filtered at a cut-off frequency of 15 Hz, before they were converted into digital signals by the A/D card with a sampling rate of 200 Hz. These signals were then converted into two Cartesian forces (normal and axial) and moments by using an A/D conversion calibration matrix. The maximum capacity of the force sensor is ±10 N (based on the range of the A/D card) with a minimum resolution of ±0.003 N (based on the noise level of the analog output signal from the digital filter). Upon completion of the calibration of the force sensor, a known weight, ranging from 0.059 N to 1.106 N, was applied at different known locations to check the accuracy of the calibration matrix. The errors in the measured forces (by the sensor) were found to be less than 2.0% of the applied weight. Since the measured hydrodynamic forces by the sensor also contained the contribution from the inertia force, the inertia term was removed using the same procedure adopted by [13]. Each set of force measurement was repeated twenty times, and the results were subsequently ensemble-averaged and then digitally smoothed, to resolve the net hydrodynamic force components. The smoothing process only accentuated but did not alter the trend of the measured forces.

III. Computational Methodology

A commercial CFD solver FULENT v15.0 was used to simulate the flow field of a flapping 2D elliptic airfoil. The accuracy and efficiency of FLUENT solver in application to flapping airfoil has been well verified and documented in the literature [16], [17]. Here, we have solved the unsteady two-dimensional Navier-Stokes equations using finite volume method (FVM) with incompressible flow assumption. The governing equations are solved in an inertial reference frame that incorporates a moving mesh following the arbitrary Lagrangian Eulerian (ALE) formulation [18]. A second order upwind scheme was applied for spatial discretization, while the time integration was performed with first-order implicit scheme. The pressure and velocity coupling was satisfied using the Pressure-Implicit with Splitting Operators (PISO) scheme [18] with a higher order approximation of the correction relation between pressure and velocity. The under-relaxation coefficients for pressure, momentum, and body force were set to 1.0. The accuracy of the solver was set to double precision, and the initial condition was maintained as the inlet uniform velocity. The convergence criterion for the adopted iterative method was satisfied with mass and momentum residuals below $O(10^{-5})$ in magnitude.

A. Problem Definition

An elliptic airfoil of thickness to chord ratio 0.125 is selected for this study which is subjected to both pitching and heaving motion. In this case, the resulting effective angle of attack profile as shown in Fig. 2 can be expressed as,

$$\alpha(t) = arcTan\left(\frac{h'(t)}{U_\infty}\right) - \theta(t) \quad (1)$$

$\alpha(t)$, U_∞, $h'(t) = dh(t)/dt$, $\theta(t)$ are instantaneous effective angle of attack of the flapping airfoil, incoming flow velocity, vertical heave velocity and instantaneous pitching angle

respectively. The Reynolds number was fixed at $Re = \rho U_\infty c / \mu = 5000$, where ρ and μ are the density and the dynamic viscosity of fluid, respectively.

$$\alpha(t) = \begin{cases} \alpha_0 Sin\left(2\pi f_1 t^*\right) & 0 \le t^* < T_K \\ \alpha_0 & T_K \le t^* < 0.5 - T_K \\ \alpha_0 Sin\left(2\pi f_1 (t^* - T_K)\right) & 0.5 - T_K \le t^* < 0.5 + T_K \\ -\alpha_0 & 0.5 + T_K \le t^* < 1.0 - T_K \\ \alpha_0 Sin\left(2\pi f_1 (t^* - 2T_K)\right) & 1.0 - T_K \le t^* < T_K \end{cases} \quad (2)$$

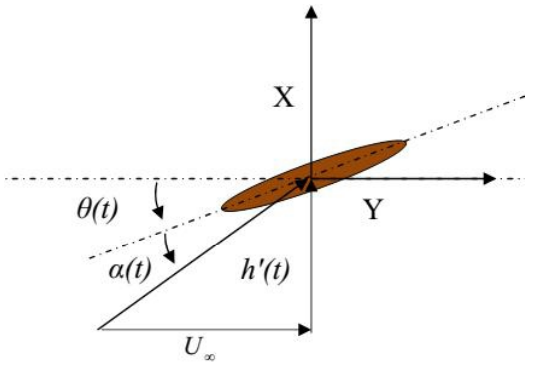

Fig. 2 Schematic drawing showing the effective angle of attack *α(t)* seen by an observer travelling with the pivot point of the airfoil

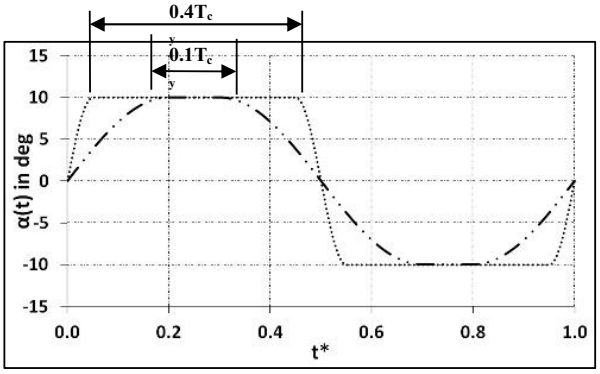

Fig. 3 Different trapezoid base length followed in the present study

TABLE I
T_K AND f_1 USED FOR DIFFERENT TRAPEZOID BASE LENGTHS

Cases	T_k	f_1
$0.4T_{cy}$	0.1	5.00
$0.3T_{cy}$	0.2	2.50
$0.2T_{cy}$	0.3	1.67
$0.1T_{cy}$	0.4	1.25

Here, we have followed *α(t)* profile as shown in (2). As shown in Fig. 3, five different base lengths of the trapezoidal *α(t)* are considered; namely $0.4T_{cy}$, $0.3T_{cy}$, $0.2T_{cy}$, $0.1T_{cy}$ and $0.0T_{cy}$ where the corresponding T_K are f_1 are shown in Table I.

In all the simulations reported here, the non-dimensional flapping cycle time T_{cy} is set to 1.0. Note that the base length of $0.0T_{cy}$ produces the smooth trapezoidal profile similar to the sinusoidal *α(t)* profile adopted by [11] and [9]. In order to maintain the smooth trapezoidal *α(t)*, only the pitching motion profile is altered using (1) while the heaving motion profile remains sinusoidal as expressed in (3):

$$h(t) = h_0 Cos(\omega t) \quad (3)$$

where h_0 is the heaving amplitude, $\omega = 2\pi f$ is the angular frequency, f is the corresponding flapping frequency, and ϕ is the phase angle between heaving and pitching motion. Only the case with $\phi = 90$ deg was considered here since this phase angle produces maximum thrust performance with better efficiency 14].

B. Computational Domain

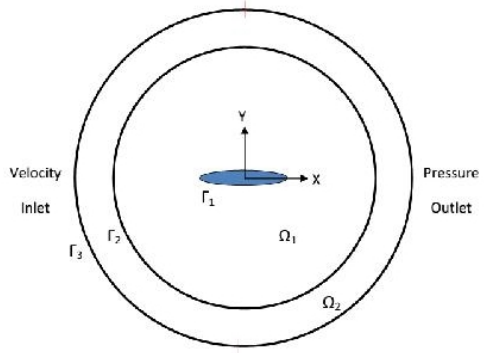

(a)

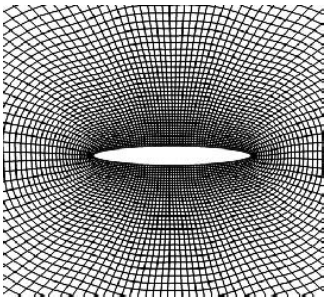

(b)

Fig. 4 (a) Schematic of O-type computational domain and (b) body conformal moving mesh around the elliptic airfoil

To analyze the thrust performance of the flapping airfoil, three different effective angles of attack amplitudes, namely α_0 = 10, 15 and 20 degrees were selected while h_0 was made constant at 0.75*c*. S_T ranged from 0.1 to 0.8 and depending on its value, the *θ(t)* is derived from (1) with a 90 deg phase difference from the corresponding heaving motion.

Lift (L) and drag (D) are defined as the component of the force normal to and parallel to the flapping motion,

respectively. The corresponding lift and drag coefficients are determined from

$$C_L = \frac{L}{0.5\rho U_\infty^2 S} \quad (4)$$

$$C_D = \frac{D}{0.5\rho U_\infty^2 S} \quad (5)$$

where S is the airfoil planform area and is set to S=1.0. The thrust coefficient C_T is obtained by computing the negative component of C_D.

In the present simulation, an O-type computational domain as shown in Fig. 4 is used. This domain consists of two zones; an inner zone Ω_1 (rotating and translating) and an outer zone Ω_2 (only translating). The elliptic airfoil Γ_1 with reference length scale c (=chord length) is located at the centre of the computational domain. The outer boundary Γ_3 is located at a radius of 30c which is sufficiently far from the airfoil and has negligible far-field boundary influence (ref. Table I). At the inlet, velocity boundary condition is defined by setting the incoming flow along X direction only, and atmospheric pressure boundary condition was applied at the outlet. A sliding interface boundary condition was enforced between the zones Ω_1 and Ω_2 to ensure time dependent momentum flux continuity across the sliding interface Ω_1 and Ω_2. Moreover, the outer boundary of Ω_1 is located at 15c, which is sufficiently far to have negligible influence on the airfoil as will be discussed later in the validation study (ref. Table II).

To ensure accurate result, high quality moving mesh is generated near the elliptic airfoil. To do this, a conformal mapping was used to create the body-conformal mesh. The intermediate boundary Γ_2 separates the inner conformal mesh (Ω_1) and the outer mesh (Ω_2). The complete inner mesh Ω_1 moved according to the airfoil kinematics, while sliding interface boundary condition maintained the flux continuity across the outer mesh Ω_2 without need to perform re-meshing.

C. Validation with Oscillating NACA0012 Airfoil

Validation was carried out using an oscillating NACA0012 airfoil subjected to simple harmonic pitching and heaving motion according to (6) and (7):

$$h(t) = h_0 Cos(\omega t) \quad (6)$$

$$\theta(t) = \theta_0 Cos(\omega t - \phi) \quad (7)$$

This flapping problem was previously investigated experimentally by [14] and later numerically by [11]. Here, we have adopted the same flow conditions, namely h_0 = 0.75c, Re = 20,000, ϕ = 90 deg and α_0 = 15 deg, and the Strouhal number was varied from 0.1 to 0.5 for validation purpose.

TABLE II
DOMAIN DEPENDENCY STUDY TO CHECK THE SIZE INFLUENCE OF REGION Ω_1 AND REGION Ω_2

Cases	Ω_1 Radius	Ω_2 Radius	Avg. C_T	% Error = $\left\lvert \frac{C_{TNewDomain} - C_{TOldDomain}}{C_{TNewDomain}} \right\rvert \times 100$
Case 1	10c	20c	0.3824	--
Case 2	15c	30c	0.3815	0.24
Case 3	20c	40c	0.3810	0.13

A computational domain was generated with a NACA0012 airfoil placed at the center of the domain. The domain dependency study was conducted to determine a suitable size of inner Ω_1 zone and outer Ω_2 zone. We have proportionately increased the radius of zone Ω_1 and Ω_2 and computed the average C_T for α_0 = 15 deg, S_T=0.3. The results are shown in Table I. Based on the insignificant error (< 0.24%) in the average C_T results, the domain size of Ω_1= 15c and Ω_2 = 30c were selected for this and subsequent simulations. Similarly, the mesh independency check were conducted to determine a suitable mesh size, and from the results presented in Table III, a mesh size with 194700 cells and 1000 time steps per cycle were selected, where the error in the average C_T is < 0.32%. The grid resolution around the airfoil up to one chord length was 13860 (198×70). This enabled the leading and trailing edge vortices to be captured with at least 1000 cells.

TABLE III
GRID INDEPENDENT STUDY TO CHECK THE INFLUENCE OF MESH SIZES

	Number of Cells	Avg. C_T	% Error = $\left\lvert \frac{C_{TNewMesh} - C_{TOldMesh}}{C_{TNewMesh}} \right\rvert \times 100$
Mesh 1	104400	0.3861	--
Mesh 2	146100	0.3824	0.99
Mesh 3	194700	0.3812	0.32
Mesh 4	239700	0.3807	0.13

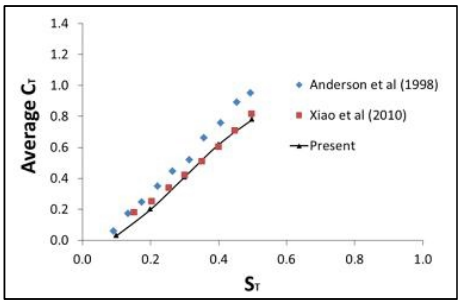

Fig. 5 Time average C_T of a NACA 0012 undergoing SHM. h_0 = 0.75c, Re = 20,000, ϕ = 90 deg and α_0 = 15 deg. Comparison with the numerical result of [11] performed under the same condition. The experimental results of [14] were obtained at a higher Re=40,000

Fig. 5 compares the time-average C_T obtained in the present simulations with the experimental results of [14] and laminar numerical simulations of [11]. It can be observed from the figure that reasonably good agreement was obtained. The slight deviation from the experimental results of [14], may be

due to the *Re* effects; the experiments were conducted at *Re*=40,000 while the present simulations carried out at *Re*=20,000. Nevertheless, both results show similar trend.

Having established the accuracy of the FLUENT v15.0 solver in capturing the flow features of flapping airfoil, we proceeded to perform the simulation, and the results are presented in the next section.

IV. Results and Discussions

In this section, we examine mean of alleviating the deterioration in the thrust performance of the oscillating airfoil at flapping frequency beyond S_{Tc}.

To verify that thrust degradation occurs when flapping frequency is above a certain critical value; we start with a case in which the elliptic airfoil is subjected to sinusoidal heaving and pitching (SHM) motion as shown in (6) and (7). The Reynolds number was maintained constant at Re=5000 while S_T ranged from 0.1 to 0.8 for three different constant peak magnitude of the effective angle of attacks (α_0), namely 10, 15 and 20 deg. The time-averaged thrust performance (C_T) is plotted in Fig. 6, which clearly indicates that the thrust performance initially increases with increasing flapping frequency. However, above a certain critical S_{Tc}, it degrades significantly for all α_0. This observation is in agreement with the findings of [9] and [11].

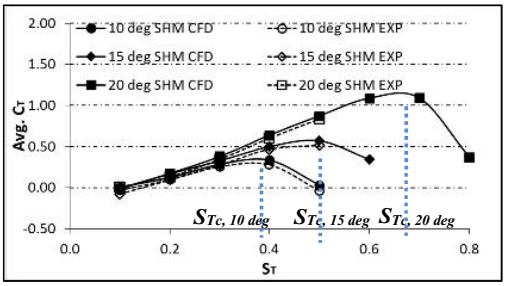

Fig. 6 Time averaged C_T for different S_T with varied α_0 (namely 10, 15 and 20 degs), where the vertical dotted lines represent S_{Tc}. The comparison between experiment and numerical results are also shown

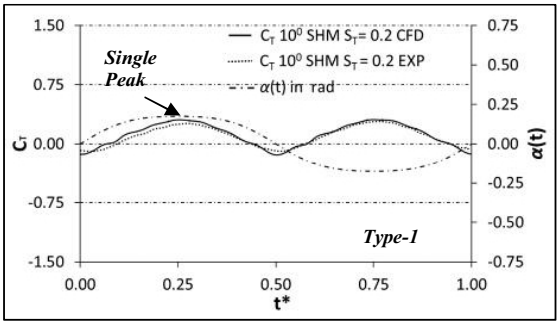

(a)

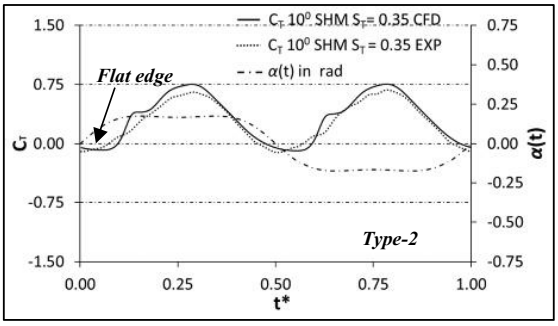

(b)

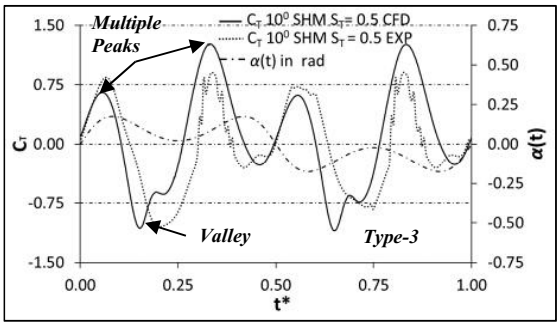

(c)

Fig. 7 Categories of transient thrust coefficient C_T and the profiles of the effective angle of attack $\alpha(t)$. (a) $\alpha_0 = 10^0$, $S_T = 0.2$, (b) $\alpha_0 = 10^0$, $S_T = 0.35$ and (c) $\alpha_0 = 10^0$, $S_T = 0.5$

In [10], it was found that as flapping frequency increases, the thrust performance of the airfoil undergoing SHM is associated with transient C_T switching from a single peak (Type-1) to a single peak with flat edge (Type-2) and then to multiple peaks (Type-3) in one flapping stroke (upstroke or downstroke) as shown in Fig. 7. The thrust deterioration when $S_T > S_{Tc}$ can be attributed to the drag producing valley in Fig. 7 (c). The associated flow physics and other details of this transient C_T profile are discussed in [10] and hence will not be repeated here for brevity. The present study focuses more on possible means of alleviating thrust deterioration when $S_T > S_{Tc}$.

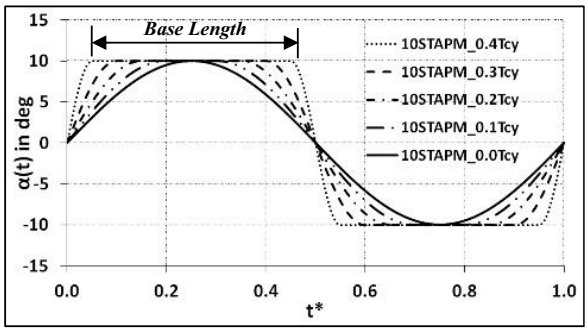

(a)

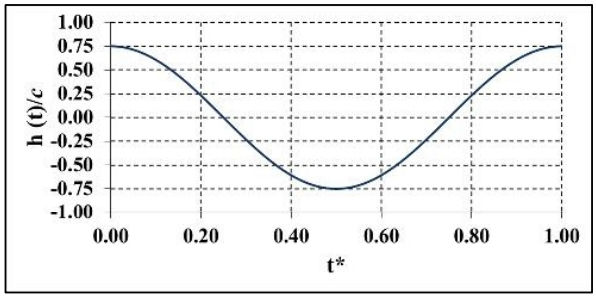

(b)

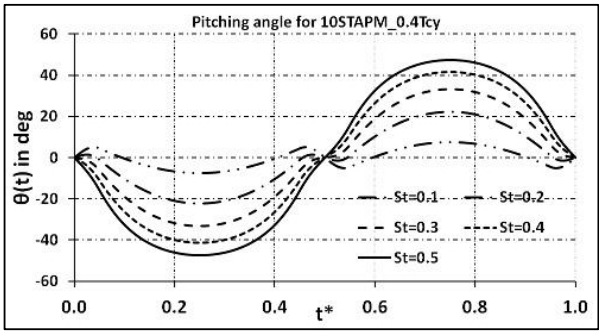

(c)

Fig. 8 (a) The effective angle of attack profiles that gradually changes from smooth trapezoidal to sinusoidal type with reduction in trapezoid base length. Here, (b) and (c) shows the sample heaving and pitching kinematics of the flapping elliptic airfoil for smooth trapezoidal effective angle of attack profile with α_0=10^0 and base length of $0.4T_{cy}$

In related past studies [9] and [11] on the 2D oscillating airfoil, it was found that the degradation in thrust performance of the airfoil subjected to SHM flapping motion beyond $S_T > S_{Tc}$ may be recovered by altering the effective angle of attack profile to square wave or cosine wave type. They associated this thrust recovery to formation of reverse von-Karman vortex street. But exactly how it affects the temporal force generation is not entirely clear.

In the present study, instead of using a square wave effective angle of attack profile, which contains infinite acceleration condition at sharp corners, we used a smooth trapezoidal effective angle of attack profile that avoids the drawbacks of the square wave. Subsequently, we reduced the trapezoid base length (see Fig. 8 (a)) until the trapezoid transforms into a sinusoidal wave. This gradual alteration in the effective angle of attack profile would help to enlighten the best thrust generating condition. As before, we used three different effective angle of attack amplitudes (α_0), namely 10, 15 and 20 deg. For a fixed heaving amplitude h_0 (= $0.75c$), constant α_0 is maintained at different S_T by adjusting the pitching amplitudes θ_0 using (1). One such sample calculated pitching angle profiles are shown in Fig. 8 (c) for the smooth trapezoidal effective angle of attack profile with α_0 = 10 deg and S_T in the range 0.1 to 0.5.

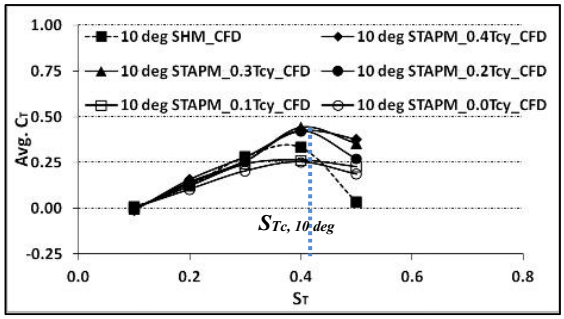

(a)

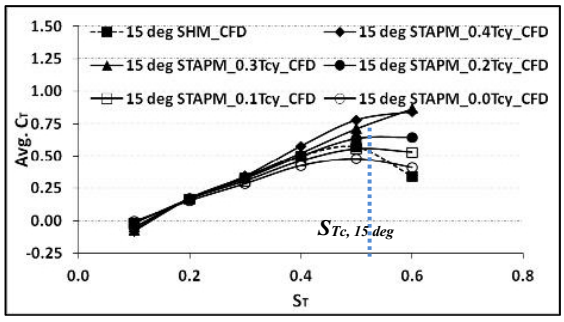

(b)

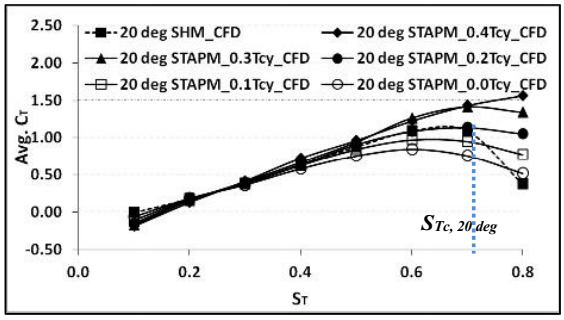

(c)

Fig. 9 Time average C_T performance as function of S_T of the elliptic airfoil for smooth trapezoidal effective angle of attack profile compared with sinusoidal heaving and pitching kinematics of the flapping airfoil for (a) α_0 = 10^0 , (b) α_0=15^0 and (c) α_0=20^0.

The time-averaged C_T of the airfoil with this smooth trapezoidal effective angle of attack profile are shown in Fig. 9 for α_0 = 10, 15 and 20 deg and at different S_T. From the figure, it can be observed that the thrust performance at low and intermediate S_T for the smooth trapezoidal is similar to that of SHM. However, at $S_T > S_{Tc}$, the thrust performance is enhanced for smooth trapezoidal effective angle of attack profiles. This observation is consistent for all α_0 considered in this study. Furthermore, the thrust performance is highest when the base length of the smooth trapezoid effective angle of attack profile is broadest i.e. for $0.4T_{cy}$. The performance decreases with the reduction in the trapezoid base length (compare C_T for $0.4T_{cy}$ to $0.0T_{cy}$ in Fig. 9).

To better understand the behavior of time-averaged C_T variation in Fig. 9, we take a closer look at the transient C_T for different values of S_T and α_0 over one flapping cycle. For the case of $\alpha_0 = 10^0$, Fig. 10 shows the transient C_T for smooth trapezoidal effective angle of attack profiles as a function of S_T during the 6th flapping cycle, when the periodic flow condition has already been established. Generally, the transient C_T profiles can be broadly categorized into three types, namely Type-1, Type-2, and Type-3. To the best of our knowledge, these characteristics have not been previously reported in the literature.

The Type-1 and Type-2 transient C_T profiles mainly occur below the critical S_{Tc} where the time-average C_T increases monotonically with S_T. The Type-1 profile is characterized by a single peak in the transient C_T variation over one flapping stroke (see Fig. 10 (a)) which is observed at low S_T. The Type-2 profile is similar to Type-1 except that it contains a flat edge just after the stroke reversal (see Fig. 10 (b)). The Type-2 pattern is observed at intermediate S_T. The Type-3 profile (see Fig. 10 (c)) differs from the other two types in that multiple peaks are observed over a given stroke at $S_T > S_{Tc}$ when the time-average C_T deteriorated (see Fig. 9). This thrust deterioration is contributed from the drag producing valley region in the transient C_T plots (see Fig. 10 (c)). Further note that the time-average thrust deterioration is less for the broad trapezoidal profile (see for the case of $0.4T_{cy}$ in Fig. 9), where the transient C_T is significantly different from the SHM (compare for the case of $0.4T_{cy}$ and SHM in Fig. 10 (c)).

Based on the trend of Type-3 transient C_T profile, we further sub-categories this type into Type-3a and Type-3b. In Type-3a, just after the stroke reversal, the transient C_T increases and attains the first peak before falling into the drag producing valley region. On the other hand, in Type-3b, after the stroke reversal, a valley region is formed which later increases to form the first peak. Moreover, Type-3b has a second valley and second peak region just before the stroke reversal (see Fig. 10 (c)). The Type-3a pattern is observed for the trapezoidal profile with a broader trapezoid base length ($>0.3T_{cy}$) as well as the SHM. On the other hand, the Type-3b pattern is observed for the trapezoidal profile with smaller trapezoid base length ($<0.3T_{cy}$). Note that for both Type-3a and Type-3b, the drag producing valley region is comparatively reduced for the smooth trapezoidal profile which results in higher time average C_T than SHM (ref. Fig. 9). Again, this drag producing region increases with increasing flapping frequency (or S_T), which further degrades the time-averaged C_T. It is worth noting that as α_0 increases, the transition of the transient C_T profiles from Type-1 to Type-2 and then to Type-3 is delayed to higher and higher S_T which further helps in thrust enchantment at higher flapping frequency or S_T.

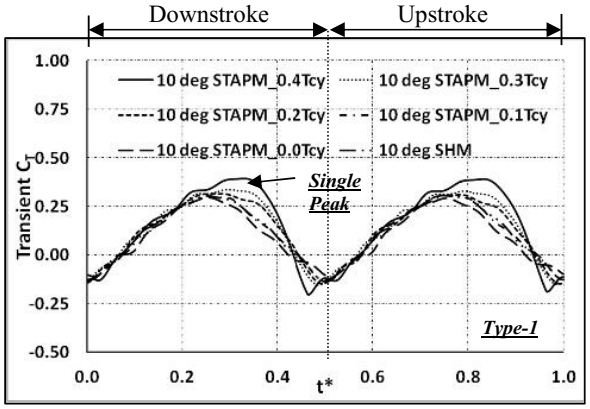

(a)

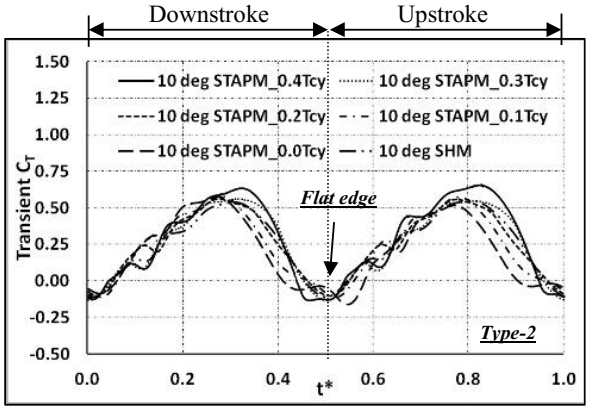

(b)

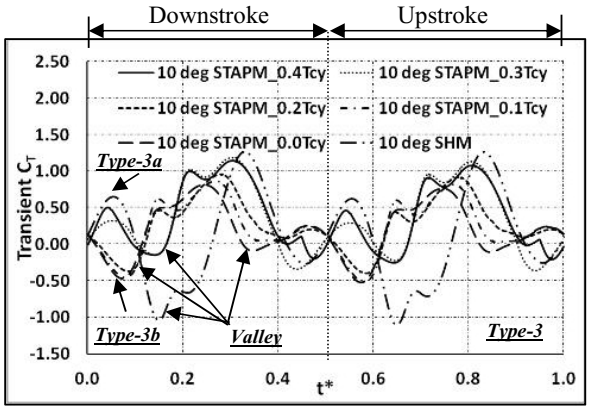

(c)

Fig. 10 Categories of the transient thrust coefficient C_T for smooth trapezoidal effective angle of attack profiles compared with SHM type flapping of the airfoil, for $\alpha_0 = 10^0$ and (a) $S_T = 0.2$, (b) $S_T = 0.3$ and (c) $S_T = 0.5$

V. Conclusions

Numerical and experimental studies have been conducted to investigate thrust performance of a 2D flapping elliptic airfoil in a forward flight condition at Re = 5000. The results show

that for all effective angle of attack profiles, higher flapping frequency produces higher time-averaged thrust C_T up to a certain critical Strouhal number (S_{Tc}); beyond which thrust generation deteriorated. The thrust deterioration can be alleviated by using a smooth trapezoidal effective angle of attack profile with a broader trapezoid base length. Furthermore, for a fixed α_0, increasing S_T to higher and higher value causes the transient C_T to switch from Type-1 (single peak) to Type-2 (single peak with flat edge) and finally to Type-3 (multiple peaks) pattern after crossing the critical Strouhal number S_{Tc}. The drag producing valley region in multiple-peak or Type-3 transient C_T pattern is mainly altered with modified smooth trapezoidal effective angle of attack profile, which subsequently bring enhancement in thrust performance.

Acknowledgment

This research work was sponsored by MOE Tier-1, Singapore academic research fund.

References

[1] C.P. Ellington, "The novel aerodynamics of insect flight: applications to micro-air vehicles," Journal of Experimental Biology, vol. 202, no. 23 pp. 3439-3448, 1999.
[2] G.C. Lewin and H. Haj-Hariri, "Modelling thrust generation of a two-dimensional heaving airfoil in a viscous flow," Journal of Fluid Mechanics, vol. 492, pp. 339-362, 2003.
[3] M.J. Smith, "Simulating moth wing aerodynamics-Towards the development of flapping-wing technology," AIAA journal, vol. 34, no.7, pp. 1348-1355, 1996.
[4] M.H. Dickinson, F.-O. Lehmann and S.P. Sane, "Wing rotation and the aerodynamic basis of insect flight," Science, vol. 284 no. 5422, pp. 1954-1960, 1999.
[5] S.P. Sane, M.H. Dickinson, "The control of flight force by a flapping wing: lift and drag production," Journal of Experimental Biology, vol. 204, no. 15, pp. 2607-2626, 2001.
[6] M.S. Triantafyllou, G.S. Triantafyllou and R. Gopalkrishnan, "Wake mechanics for thrust generation in oscillating foils," Physics of Fluids A, vol. 3, no. 12, pp. 2835-2837, 1991.
[7] G.S. Triantafyllou and M.S. Triantafyllou, M.A. Grosenbaugh, "Optimal Thrust Development in Oscillating Foils with Application to Fish Propulsion," Journal of Fluids and Structures, vol. 7, no. 2, pp. 205-224, 1993.
[8] D.A. Read, F.S. Hover and M.S. Triantafyllou, "Forces on oscillating foils for propulsion and maneuvering," Journal of Fluids and Structures, vol. 17, no. 1, pp. 163-183, 2003.
[9] F. Hover, Ø. Haugsdal and M. Triantafyllou, "Effect of angle of attack profiles in flapping foil propulsion," Journal of Fluids and Structures, vol. 19, no. 1, pp. 37-47, 2004.
[10] S.M. Dash, K.B. Lua and T.T. Lim, "On the thrust performance of a 2D flapping foil in a forward flight condition," Bulletin of the American Physical Society, 60 (2015).
[11] Q. Xiao and W. Liao, "Numerical investigation of angle of attack profile on propulsion performance of an oscillating foil," Computers & Fluids, vol. 39, no. 8, pp. 1366-1380, 2010.
[12] J. Abolfazli Esfahani and H.R. Karbasian, "Comparative investigations in the effect of angle of attack profile on hydrodynamic performance of bio-inspired foil," Journal of Naval Architecture and Marine Engineering, vol. 10, no. 2, pp. 99-108, 2013.
[13] K. Lua, T. Lim and K. Yeo, "Effect of wing–wake interaction on aerodynamic force generation on a 2D flapping wing," Experiments in Fluids, vol. 51, no. 1, pp. 177-195, 2011.
[14] J. Anderson, K. Streitlien, D. Barrett and M. Triantafyllou, "Oscillating foils of high propulsive efficiency," Journal of Fluid Mechanics, vol. 360, pp. 41-72, 1998.
[15] K. Lua, T. Lim, K. Yeo and G. Oo, "Wake-structure formation of a heaving two-dimensional elliptic airfoil," AIAA journal, vol. 45, no. 7, pp. 1571-1583, 2007.
[16] F.M. Bos, D. Lentink, B. Van Oudheusden and H. Bijl, "Influence of wing kinematics on aerodynamic performance in hovering insect flight," Journal of Fluid Mechanics, vol. 594, pp. 341-368, 2008.
[17] J.-J. Lee, C.-T. Hsieh, C.C. Chang and C.-C. Chu, "Vorticity forces on an impulsively started finite plate," Journal of Fluid Mechanics, vol. 694, pp. 464-492, 2012.
[18] J.H. Ferziger and M. Perić, "Computational methods for fluid dynamics," Springer Berlin, 2002.